Supplementary Information for

Harnessing transition waves to realize deployable structures

Ahmad Zareei, Bolei Deng, and Katia Bertoldi

Corresponding Author: Katia Bertoldi
John A. Paulson School of Engineering and Applied Sciences
Harvard University, Cambridge, MA 02138, USA
E-mail: bertoldi@seas.harvard.edu

This PDF file includes:

Figs. S1 to S4
Captions for Movies S1 to S5
References for SI reference citations

Other supplementary materials for this manuscript include the following:

Movies S1 to S5

1. Numerical Model

To get a better understanding of the propagation of transition waves in our linkages, we develop a numerical model. In our numerical simulations we model the links as rigid bodies of mass m (note that m includes the mass of the link as well as the pins, screws and bolts used at the joints), length L, and moments of inertia I. We assume that the structure deforms in the (x, y) plane and use (x_i, y_i) and α_i to denote the position of the center of mass and of the i-th link and the angle between the i-th link and the horizontal direction, respectively (Fig. S1a). We then connect the i-th link to its $i \pm q$ neighbor via a linear spring with stiffness $k^{(q)}$, rest length $l^{(q)}$ and current length $l_{i,i\pm q}$ given by

$$l_{i,i\pm q} = \sqrt{(x_i + d\sin\alpha_i - x_{i\pm q} - d\sin\alpha_{i\pm q})^2 + (y_i - d\cos\alpha_i - y_{i\pm q} + d\cos\alpha_{i\pm q})^2}. \quad \text{[S1]}$$

where d is the vertical off-set between the line connecting the center of joints and the line connecting the springs. Further, to ensure that subsequent links stay connected and that $0 \le \theta_i \le \Theta$ (where $\theta_i = \alpha_{i+1} - \alpha_i$ is the i-th joint angle), we introduce three elastic springs at each joint: (i) a linear spring with stiffness $k_x = 50k^{(q)}$; (ii) a linear spring with stiffness $k_y = 50k^{(q)}$ and (iii) a non-linear rotational spring with stiffness k_θ defined as

$$k_\theta = \begin{cases} 50k^{(q)}L & \theta_i < 0 \text{ or } \theta_i > \Theta \\ 0 & 0 \le \theta_i \le \Theta \end{cases} \quad \text{[S2]}$$

Under these assumptions, the Lagrangian of a linkage chain comprising n units can be written as

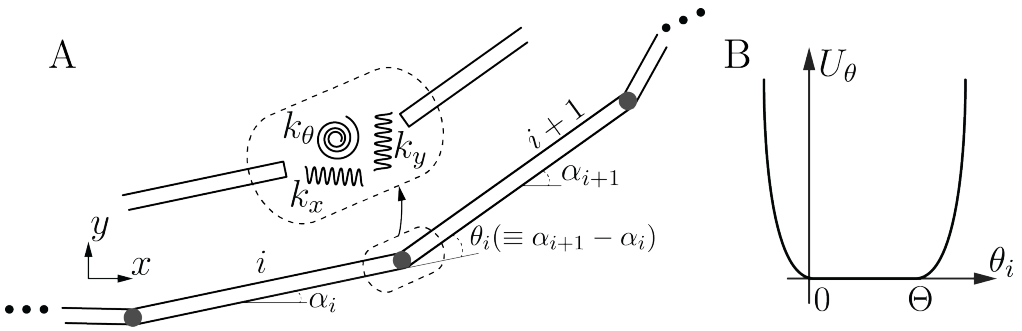

Fig. S1. (a) Schematic of the linkage mechanism where each link is considered as a bar with total mass m and moment of inertia I. The inset figure shows that the joints are replaced with two stiff horizontal/vertical springs with stiffness k_x,k_y and a nonlinear torsional spring k_θ. (b) The nonlinear torsional spring potential function U_θ versus joint angle θ_i. The potential U_θ is zero when $\theta_i \in [0, \Theta]$ and quadratic in theta otherwise.

$$\mathcal{L} = T - U = \sum_{i=1}^{n} T_i - \sum_{i=1}^{n-q} U_i^{(q)} - U_{\text{const.}} \quad \text{[S3]}$$

where T_i is the kinetic energy of i-th link,

$$T_i = \frac{1}{2}m(\dot{x_i}^2 + \dot{y_i}^2) + \frac{1}{2}I\dot{\alpha_i}^2, \quad \text{[S4]}$$

$U_i^{(q)}$ is the potential energy stored in the spring connecting the i-th and $(i+q)$-th links

$$U_i^{(q)} = \frac{1}{2}k^{(q)}\left(l_{i,i+q} - l_0^{(q)}\right)^2, \quad \text{[S5]}$$

[S6]

and $U_{\text{const.}}$ is the energy associated to the constraints introduced at the joints to ensure that subsequent links stay connected and that $0 \leq \theta_i \leq \Theta$

$$U_{\text{const.}} = \sum_{i=2}^{n} \frac{1}{2} k_x (x_i - \frac{L}{2}\cos\alpha_i - x_{i-1} - \frac{L}{2}\cos\alpha_{i-1})^2 + \sum_{i=2}^{n} \frac{1}{2} k_y (y_i - \frac{L}{2}\sin\alpha_i - y_{i-1} - \frac{L}{2}\sin\alpha_{i-1})^2 + \sum_{i=1}^{n-1} U_\theta(\theta_i) \quad \text{[S7]}$$

with

$$U_\theta(\theta_i) = \begin{cases} \frac{1}{2} k_\theta (\theta_i - \Theta)^2 & \theta_i > \Theta \\ 0 & 0 \leq \theta_i \leq \Theta \\ \frac{1}{2} k_\theta \theta_i^2 & \theta_i \leq 0 \end{cases} \quad \text{[S8]}$$

The discrete equations of motion for the i-th link are then obtained via the Euler–Lagrange equations as

$$\begin{aligned}
m\ddot{x}_i = &-k_x(x_i - \frac{L}{2}\cos\alpha_i - x_{i-1} - \frac{L}{2}\cos\alpha_{i-1}) - k_x(x_i + \frac{L}{2}\cos\alpha_i - x_{i+1} + \frac{L}{2}\cos\alpha_{i+1}) \\
&- k^{(q)} \frac{x_i - x_{i+q} + d\,(\sin\alpha_i - \sin\alpha_{i+q})}{l_{i,i+q}} \left(l_{i,i+q} - l_0^{(q)}\right) \\
&- k^{(q)} \frac{x_i - x_{i-q} + d\,(\sin\alpha_i - \sin\alpha_{i-q})}{l_{i,i-q}} \left(l_{i,i-q} - l_0^{(q)}\right) \\
m\ddot{y}_i = &-k_y(y_i - \frac{L}{2}\sin\alpha_i - y_{i-1} - \frac{L}{2}\sin\alpha_{i-1}) - k_y(y_i + \frac{L}{2}\sin\alpha_i - y_{i+1} + \frac{L}{2}\sin\alpha_{i+1}) \\
&- k^{(q)} \frac{y_i - y_{i+q} - d\,(\cos\alpha_i - \cos\alpha_{i+q})}{l_{i,i+q}} \left(l_{i,i+q} - l_0^{(q)}\right) \\
&- k^{(q)} \frac{y_i - y_{i-q} - d\,(\cos\alpha_i - \cos\alpha_{i-q})}{l_{i,i-q}} \left(l_{i,i-q} - l_0^{(q)}\right) \\
I\ddot{\alpha}_i = &-k_x \frac{L}{2}\sin\alpha_i(x_i - \frac{L}{2}\cos\alpha_i - x_{i-1} - \frac{L}{2}\cos\alpha_{i-1}) + k_x \frac{L}{2}\sin\alpha_i(x_i + \frac{L}{2}\cos\alpha_i - x_{i+1} + \frac{L}{2}\cos\alpha_{i+1}) \\
&+ k_y \frac{L}{2}\cos\alpha_i(y_i - \frac{L}{2}\sin\alpha_i - y_{i-1} - \frac{L}{2}\sin\alpha_{i-1}) - k_y \frac{L}{2}\cos\alpha_i(y_i + \frac{L}{2}\sin\alpha_i - y_{i+1} + \frac{L}{2}\sin\alpha_{i+1}) \\
&- k^{(q)} \frac{d\cos\alpha_i\,[x_i - x_{i+q} + d(\sin\alpha_i - \sin\alpha_{i+q})]}{l_{i,i+q}} \left(l_{i,i+q} - l_0^{(q)}\right) \\
&- k^{(q)} \frac{d\cos\alpha_i\,[x_i - x_{i-q} + d(\sin\alpha_i - \sin\alpha_{i-q})]}{l_{i,i-q}} \left(l_{i,i-q} - l_0^{(q)}\right) \\
&- k^{(q)} \frac{d\sin\alpha_i\,[y_i - y_{i+q} + d(\cos\alpha_i - \cos\alpha_{i+q})]}{l_{i,i+q}} \left(l_{i,i+q} - l_0^{(q)}\right) \\
&- k^{(q)} \frac{d\sin\alpha_i\,[y_i - y_{i-q} + d(\cos\alpha_i - \cos\alpha_{i-q})]}{l_{i,i-q}} \left(l_{i,i-q} - l_0^{(q)}\right) - U'_\theta(\alpha_i - \alpha_{i-1}) + U'_\theta(\alpha_{i+1} - \alpha_i)
\end{aligned} \quad \text{[S9]}$$

Next, to account for the energy dissipation due to the sliding of the structure on the surface, we add to Coulomb friction terms of type $-\mu m g \dot{x}_i/(\dot{x}_i^2 + \dot{y}_i^2)$ and $-\mu m g \dot{y}_i/(\dot{x}_i^2 + \dot{y}_i^2)$ ($\mu = 0.2$ being the experimentally measured coefficient of friction between the structure and the surface). Further, subsequent links do not oscillate back and forth when their angle reaches 0 or Θ, we also include a dissipation term in the form of $c\dot{\theta}$ (with $c/L\sqrt{mk^{(q)}} = 4$) that is only activated when $\theta_i < 0/\ \theta_i > \Theta$. Finally, since in all experiments the linkages are placed on a flat surface in the $x - y$ plane with a wall located at $y = 0$ and aligned along the

x-direction that limits motion in y-direction, we introduce a wall-type potential U_y defined as

$$U_y(y) = \begin{cases} 0 & y \geq 0, \\ \frac{1}{2} 50 k^{(q)} y^2 & y < 0. \end{cases} \quad [S10]$$

We numerically solve Eqs. (S9) using Runge–Kutta fourth order method with time-steps $\delta t = 0.01\,\text{sec}$. As in the experiments, in all simulations we clamp the first link by setting $x_1 = y_1 = 0$, and $\alpha_1 = 0$. The pulse is then initiated by imposing

$$\dot{\alpha}_1(t=0) = \sqrt{\frac{2U_{\text{per}}}{I_1}}, \quad [S11]$$

where U_{per} is the energy of the applied perturbation , which can be estimated from the experimentally measured initial (i.e. at $t = 0$) linear ($\mathbf{v}_1\big|_{t=0}$) and angular velocities of the first link as

$$U_{\text{per}} \equiv T_1(t=0) = \frac{m}{2}\left(\dot{x}_1^2 + \dot{y}_1^2\right)\Big|_{t=0} + \frac{I}{2}\dot{\alpha}^2\Big|_{t=0}. \quad [S12]$$

Additional numerical results

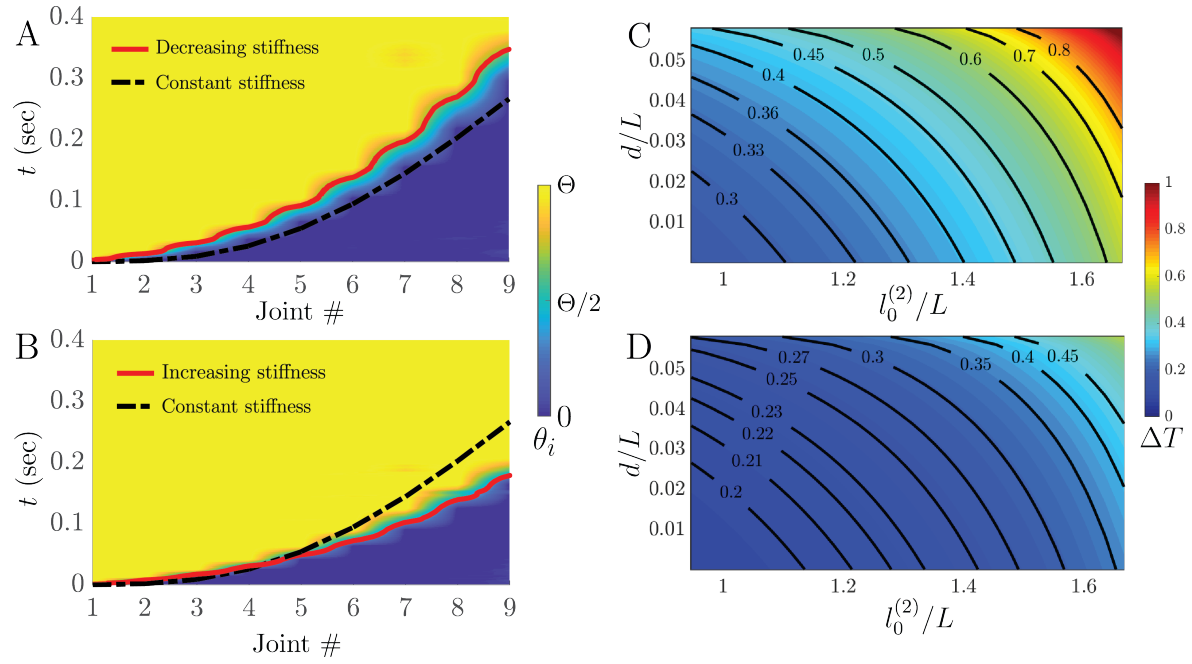

Fig. S2. While in the main text we show numerical results for linkages with spatially constant properties, here we report numerical predictions for linkages with next-nearest neighbors springs of spatially increasing and decreasing stiffness. Specifically, we consider a linkage for which the stiffness of the i-th spring is $k_i^{(2)} = k^{(2)} + 4(i-1)k^{(2)}/7$ and one for which $k_i^{(2)} = k^{(2)} - (i-1)k^{(2)}/28$. (A)-(B) The normalized angle of the individual bistable joints (θ for each of the joints in the linkage) during the propagation of the transition wave in a linkage with $d/L = 0.02$, $l_0^{(2)}/L = 1.64$, $U_{\text{per}}/U_0^{(2)} = 0.5$ and spring with spatially (A) increasing and (B) decreasing stiffness. In both plots the dashed black line indicates the wavefront predicted by the numerical simulations for a linkage realized with spring of identical stiffness. (C)-(D) Theoretically predicted evolution of the time it takes for the transition wave to reach the last joint, ΔT, as a function of the geometrical parameters d/L and $l_0^{(2)}/L$ for linkages with with spatially (C) increasing and (D) decreasing stiffness. All these numerical results indicate that the velocity profile of the supported transition waves can be manipulated by varying the stiffness of the connecting springs along the structure.

2. Experiments

A. Fabrication. To realize linkages with bistable joints, we start by designing rigid bars of length L that allow each joint to rotate between 0 and Θ. This is achieved using the design shown in Fig. S3(a). Note

that the triangular feature at the top of the links prevent rotations larger that Θ, while the small step at their bottom stops the rotation at $\theta = 0$ (see Fig. S4). Moreover, three circular holes are embedded in each link: the two closed to the ends are used to connect to the neighboring elements via pins, whereas the one in the middle (which is at a distance d from the line connecting the center of the other two holes) is used to connect the springs to the bar using screws and bolts. Each bar is fabricated out of four layers of plexi-glass with thickness of 3 mm. The laser-cut layers are glued together as shown in Fig. S3(b) to form a link.

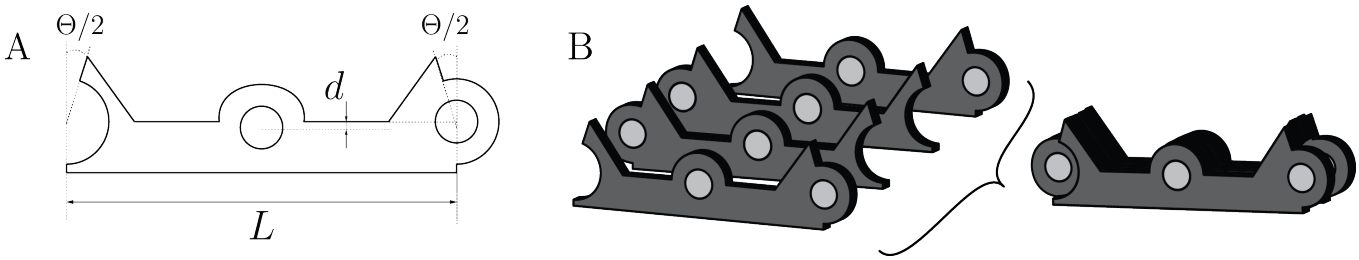

Fig. S3. (a) Schematic of a single layer of our bar. (b) A bar is constructed by gluing four layers together.

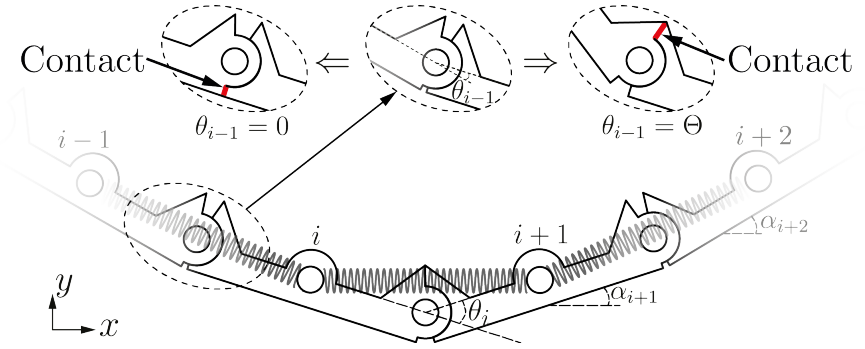

Fig. S4. Schematic of the structure. Inset figures highlight the contact points when a joint's angle is at 0 or Θ.

The total mass of each link is $m = 16.3$ g for nearest neighbor connections and $m = 18.8$ g for next-nearest-neighbor connections and accounts for the mass of the plexi-glass layers ($m_{\rm pg}$=8.6 g), pins ($m_{\rm p}$=1.1 g), springs ($m_s^{(1)}$=2×2.2 g for nearest-neighbor and $m_s^{(2)}$=6.9 g for next-nearest-neighbor connections) and screw and bolts ($m_{\rm sb}$=2.2 g). The moment of inertia for each link is calculated by considering the link as a rigid rod of length L and mass $m_{\rm pg} + m_s$ (note that we neglect the complex shape of the link) and considering the pins, screws, and bolts as point masses. It follows that the moment of inertia of each unit with respect to its center of mass is

$$I = \frac{m_{\rm pg} + m_s}{12} L^2 + m_{\rm p} \left(\frac{L}{2}\right)^2 . \qquad \text{[S13]}$$

The springs used in our linkage with nearest neighbor connections have stiffness $k^{(1)} = 2 \times 507.86$ N/m and rest length $l_0^{(1)} = 38.09$ mm (McMaster-Carr product id: 9044K125), whereas those used to construct the linkage with the next-nearest neighbor have stiffness $k^{(2)} = 753.53$ N/m and rest length $l_0^{(2)} = 82.55$ mm (McMaster-Carr product id: 9044k168), as reported by the manufacturer (https://www.mcmaster.com/9044k125 and https://www.mcmaster.com/9044k168). All the springs are stretched when the linkage is in its initial, straight configuration, resulting in an initial force of 12.10 N and 13.14 N for the nearest-neighbor and next-nearest-neighbor connections, respectively.

B. Testing. In all our tests, we place the linkages in the straight configuration on a flat surface in the $x-y$ plane (note that gravity acts in the z direction), clamp their right end and apply a pulse in the y-direction to left most link. We monitor the propagation of the excited transition waves with a high-speed camera (SONY RX100) recording at 480 fps. To extract the required information from the recorded movies, we use the open source Python image processing library OpenCV (1) and track the position of green markers attached to the center of each bar. More specifically, we first use Morphological transformation of erosion followed by dilation (i.e., MORPHOLOGYEX) with a kernel size of 7 pixels to remove the noise in the image. Then, we transform the image to gray color space, convolve the image with a normalized box filter of size 3, and use thresholding to isolate the green pixels.

Movie S1. Propagation of a transition wave in a bistable linkage with nearest neighbor connections. the wave is initiated by applying a perturbation to the first bar characterized by $U_{\mathbf{per}}/U_0^{(1)} = 0.5$.

Movie S2. Propagation of a transition wave in a bistable linkage with nearest neighbor connections. the wave is initiated by applying a perturbation to the first bar characterized by $U_{\mathbf{per}}/U_0^{(1)} = 2.67$.

Movie S3. Propagation of a transition wave in a bistable linkage with next-nearest neighbor connections. the wave is initiated by applying a perturbation to the first bar characterized by $U_{\mathbf{per}}/U_0^{(2)} = 0.47$.

Movie S4. Propagation of a transition wave in a structure created by coupling two linkages with next-to-nearest neighbor connections. The pulse transforms the initially flat structure into a profile with changing concavity.

Movie S5. Propagation of a transition wave in a structure comprising four linkages characterized by $d/L = 0.02$ and $\Theta = \pi/10$. The springs enable the transfer of the waves from one linkage to the other and, ultimately, the deployment of the 3D dome-like structure.

References

1. Bradski G (2000) The OpenCV Library. *Dr. Dobb's Journal of Software Tools*.